Split-pane electrochromic window control based on an embedded photometric device with real-time daylighting computing

Yujie Wu[a,*], Taoning Wang[b], Eleanor S. Lee[b], J´er omeˆ H. K¨ampf[c], Jean-Louis Scartezzini[a]

[a] *Solar Energy and Building Physics Laboratory (LESO-PB), Ecole polytechnique f´ed´erale de Lausanne (EPFL), CH-1015, Lausanne, Switzerland*

[b] *Building Technology and Urban Systems Division, Energy Technologies Area, Lawrence Berkeley National Laboratory, Mailstop 90-3111, 1 Cyclotron Road, Berkeley, California 94720, USA*

[c] *Idiap Research Institute, CH-1920, Martigny, Switzerland*

Abstract

Well-designed electrochromic (EC) glazing control can improve the energy performance of buildings and visual comfort of occupants in highly glazed buildings. This paper designed and demonstrated a compact integrated EC glazing automation system to control tint states of a split-pane EC window according to variations of sky conditions. The control is based on monitoring the luminance distribution of the sky and real-time lighting computation for a building interior, using an embedded photometric device (EPD). It optimizes tint states of EC glazing to offer sufficient daylight provision and temper discomfort glare for occupants, which potentially mitigates excessive solar heat gain. 'In-situ' experiments were conducted in a full-scale testbed to demonstrate the daylighting performance under various sky conditions. Experimental results showed 83% of the working time for work-plane illuminance (WPI) and 95% of the time for daylight glare probability (DGP) were constrained in comfort range (WPI∈[500, 2000] lux, DGP ≤ 0.35) by the automated EC glazing (controlled by EPD) under clear skies; 68% of the time for WPI and 94% of the time for DGP in confined range under clear skies with thin clouds; 62% of the time for WPI and 85% of the time for DGP in confined range under partly cloudy skies.

Keywords: Electrochromic window; Real-time lighting simulation; FPGA; Embedded photometric system; Visual comfort; HDR imaging

1. Introduction

Strategies for regulating daylight in buildings have been actively applied to mitigate energy consumption and promote visual comfort for occupants. The growing adoption of highly glazed facadesin modern office buildings enhances the availability of daylight and exterior view for occupants [1, 2]. Although daylight exploitation can reduce heating load and demand for electric lighting, excessive daylight ingress not only contributes to the upsurge of cooling load in a warm climate [3] but also induces discomfort glare for occupants, which can be moderated by daylighting control [4]. Research on visual comfort has gradually unveiled daylight contribution to occupants' health [5] and productivity [6]. The productivity saving of occupants, if projected on staffs' salaries benefits, is estimated to significantly exceed energy bills in office buildings [7, 8]. Despite its subjective notion, visual comfort has been quantified by multiple daylight metrics and norms for assessment according to levels of occupants' satisfactory, from the perspectives of daylight provision and discomfort glare sensation. The European standard on lighting (EN 12464) [9] stipulates the minimum work-plane illuminance (WPI) required for different indoor activities, including 500 lux for reading and writing, 1000 lux for quality control and inspection, and 1500 lux for precise manufacturing tasks. WPI lower than 500 lux can also be regarded as sufficient lighting for certain activities including computer-based work [10]. Studies have also found occupants have different preferences on the illuminance levels possibly due to their distinct sensitivity to light [11] and can tolerate lower illuminance levels of daylight than that of artificial light [12]. The recent European standard on daylighting of buildings (EN 17037) [13] contains outwards view assessment ratings for occupants. Multiple glare risk metrics have been proposed for daylit environments for evaluating occupant discomfort glare, including the Daylight Glare Probability (DGP) [14] and the Daylight Glare Index (DGI) [15]. A number of studies have validated DGP as a reliable index for assessing glare risk in daylit space according to levels of occupant discomfort [16, 17]. These norms and metrics have paved the way for researchers and designers to improve the visual comfort of occupants.

Shading devices are commonly applied in conjunction with facadesto tune daylight injection into buildings. Although exterior shad-ing devices can achieve low heat gain and are relatively inex-pensive to manufacture [18], switchable glazing preserves exte-rior views for occupants and has less installation, durability, and maintenance issues compared to shading devices [19]. It has

*Corresponding author at: Solar Energy and Building Physics Laboratory (LESO-PB), Ecole polytechnique f´ed´erale de Lausanne (EPFL), CH-1015, Lausanne, Switzerland

Email address: yujie.wu@epfl.ch (Yujie Wu)

been used as an alternative product for regulating daylighting in highly glazed office buildings, to improve energy saving and visual comfort. With its technological advances, electrochromic (EC) glazing, which can change its optical property under an applied voltage, features multiple merits for building applications, including a high modulation range of light transmittance, low driving voltage, and clear view in all tint states [20], as compared to crystal liquid and suspended particle devices.

The integration of EC glazing with a control system is a major challenge for the broad application of EC windows. Since the sky is dynamic, daylight conditions can change drastically dur-ing daytime according to variations in the sun position, atmo-sphere turbidity, and patterns and motion of clouds. If not har-nessed properly, excessive daylight fluxes can overheat building interior and simultaneously induce discomfort glare for occu-pants [21]. Tint states of EC glazing therefore must vary in real-time according to dynamic sky conditions to optimize day-lighting in building interior, which is impractical to be realized by manual manipulation [22, 23]. Well-designed daylight con-trol systems can substantially reduce peak cooling loads, pro-vide sufficient daylight, and improve occupants' visual comfort [24]. Early studies of EC glazing control systems focused on maintaining the daylight provision with a single tint state of the whole window. Sullivan et al. [25] simulated three strategies of EC glazing control to compare their energy performance, in-cluding work-plane illuminance (WPI) maintenance based on a closed-loop control, linear tuning based on incident solar radi-ation and set-points, and tint control according to the cooling load. From the energy saving perspective, Karlsson et al. [26] studied control of EC transmittance according to solar radia-tion impinging on the window surface in three different loca-tions. Lee et al. [27] employed a ceiling-mounted photo-sensor to monitor WPI, based on which a closed-loop control system was set-up to maintain WPI between 540 and 700 lux. Daily lighting electricity demand was reduced by 8-23% as compared to a reference tinted glazing showing luminous transmittance of 0.5. Despite the achieved savings in artificial lighting by main-taining sufficient daylighting, the lighting control strategies can also influence the lighting saving in a specific application [28].

Recent studies of EC glazing control have started taking dis-comfort glare into consideration as a human centric control in order to improve visual comfort for occupants. Jonsson et al. [29] constrained the transmitted direct solar vertical irradiance below 200 W/m^2 to moderate discomfort glare in a simulation study. Gugliermetti et al. [30] used DGI to determine a so-lar irradiance set point to mitigate discomfort glare. Piccolo et al. [31] employed two metrics, DGI_N [32] and Glare Subjec-tive Rating (SR) [33], to assess glare moderation by a closed-loop system that maintained WPI at approximately 300 lux. Al-though these approaches can improve visual comfort in a given situation, they are not designed to precisely control discomfort glare for users at a specific location (user-centric control); im-precise daylight control can either turn the environment dark [34], increasing usage of artificial lighting [35], or moderate glare insufficiently. Preventing discomfort glare from the sun remains a difficult task when the sun is in the field of view (FOV) of occupants. Fernandes et al. [36] introduced split-pane EC glazing control in which transmittance of two window panes was controlled independently. In order to moderate dis-comfort glare, two metrics (vertical illuminance at the eye level of occupants and luminance ratio between a visual task area and surrounding environment) were controlled by using the lighting calculation based on weather data and sky luminance models. In another study, Fernandes et al. [37] performed EC glazing control with different modes according to the set points of out-door vertical illuminance and solar position that is calculated based on astronomical formulas. When the sun is within a pre-set position range (can be seen through a window by occupants at a defined position), one or more subpanes will be tinted to the darkest state to temper discomfort glare, despite the result-ing dark daylit environment as reported by occupants. The set-points were changed seasonally to achieve better performance of glare mitigation in contrast to the adoption of constant set-points. Although discomfort glare from direct sun exposure can be improved by the adjustment of set-points based on practi-tioners' experience, the issue of veiling glare remains a chal-lenge due to secondary reflections on specular surfaces from the exterior surroundings, including glazing facades of oppo-site buildings and windscreen of parked vehicles. With tech-nological advances, calibrated cameras have been used indoors to monitor discomfort glare of occupants and control shading accordingly [38]. However, privacy issues introduced by plac-ing cameras within buildings to monitor interior space remains an impeding factor for a real application in EC window control [39]. Furthermore, since tinted EC glazing renders a bluish en-vironment and it is believed that users have a preference on the neutral spectrum of daylighting, Mardaljevic et al. [40] studied an approach for maintaining the neutral spectrum of illumina-tion with an EC window by combining tinted glazing panels with a small portion of clear glazing panels.

In this paper, a highly integrated EC glazing automation sys-tem was designed and 'in-situ' experiments were performed to demonstrate the maintenance of daylight provision and mitiga-tion of discomfort glare for occupants. The imaging system of the controller, attached to an EC window, monitors lumi-nance distribution in the exterior space, to avoid privacy is-sues in buildings. Based on a monitored luminance map, the controller is able to perform real-time lighting calculations and control tint states of an EC window to temper discomfort glare. Design of the decentralized system is introduced in Section 2. The computation method and control algorithms are explained in Section 3. The empirical validation results are presented in Section 4 with regard to the performance of EC glazing con-trol.

2. Design

2.1. Systematic design of the automated EC glazing

The design of the automated EC glazing integrates an embed-ded photometric device (EPD) [41] that is attached on the glass,

with its imaging system targeted towards outdoors as illustrated in Figure 1, to control glazing tints to improve visual comfort for occupants, as a stand-alone system. The EPD acts as both a sensing unit and a controller for the EC glazing. With a vision of outdoor space, the EPD monitors luminance distribution of the sky vault and landscape faced by the fac¸ade, including the sun, clouds, sky background, and landscape objects. Based on a generated luminance map together with a geometric model of the building interior, EC tint states are determined based on the real-time lighting simulation performed on the EPD. It evalu-ates work-plane illuminance (WPI) and glare risk for various combinations of glazing tint, and the optimal tint state is de-termined to offer sufficient daylight provision and minimal dis-comfort glare for occupants within the building interior. The highly integrated design enhances convenience during installa-tion and application, since sensors or wiring connections are not required within the building interior. Privacy issues of us-ing cameras with vision of a building interior are avoided, since the imaging system of the EPD targets the outdoor space. Fur-thermore, the circuitry of an EPD is compatible with that of an EC glazing driver, since both are driven by low DC (direct-current) voltage, which can be integrated on a single printed circuit board (PCB).

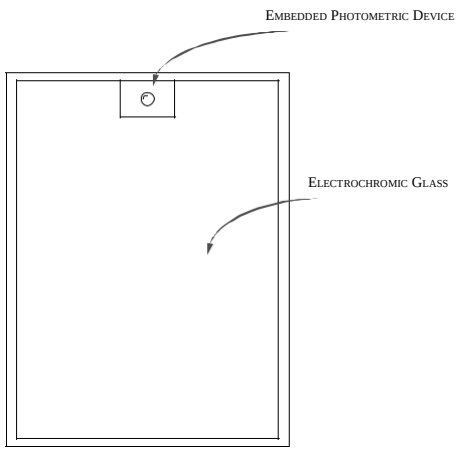

Fig. 1. Design of an EC glazing integrated with an EPD (view from the outdoors towards the glazing surface)

2.2. *Embedded photometric device*

The EPD, proposed and demonstrated by Wu et al. [41, 42], mainly comprises a low-cost image sensor, lens, and a field pro-grammable gate array (FPGA) processor. The imaging system of the EPD was deliberately calibrated in the spectral response, vignette effect, signal response curves, and geometric mapping. After spectral correction by optical filters, the spectral response of the imaging system matched the CIE photopic luminosity function V(λ) [43], which emulates the response of human eyes. The spectral correction error f_1' reaches 8.89% for photometric variable measurements. Based on its fast shutter speed, the EPD has a wide range of luminance detection from 120 cd/m^2 to 3.78×10^9 cd/m^2 (150 dB) based on HDR imaging techniques, which covers both the luminance of shadowed landscape during daytime and that of the direct sun orb ($\leq 1.6 \times 10^9$ cd/m^2) as the two extremes. The EPD monitors the luminance distribution of the sky vault and landscape, within a 1.3 second acquisition time, and generates a luminance map with 1.2 million patches. In conjugation with a modelled scene, the real-time daylighting simulation can be performed on the EPD to assess indoor light-ing conditions. Based on a high-resolution luminance map, the capability of lighting simulation on the EPD was validated in several studies for facadeswith clear glazing and blinds in Lau-sanne, Switzerland [44, 45] which achieved below 20% error in simulating WPI distribution under dynamic sky conditions.

3. Methodology

3.1. *Daylighting testbed*

The space selected for this study is a full-scale outdoor testbed (Advanced Windows Testbed, Building 71t) with three parallel office rooms located at the Lawrence Berkeley National Labora-tory (LBNL) in Berkeley, CA (37°52′34.2″N, 122°14′59.9″W). The three rooms are designated as Room A, B, and C, with Room A to the east, Room B in the center, and Room C to the west, from right to left as shown in Figure 2 a). The dimen-sion of each office room is 3 × 4.5 × 3.3 m^3, furnished with an identical interior set-up and a south facing unilateral fac¸ade showing a 0.64 window-to-wall ratio. Each fac¸ade of the two rooms (Room B and C) is equipped with a split-pane EC glaz-ing, of which the upper daylight section and lower view section can be controlled independently. The EC glazing (from Sage Glass) has four states of luminous transmittance: 60% (clear), 18% (light tint), 6% (medium tint), and 1% (full tint). It takes 10 ~ 30 min for transition from the clear (60% transmittance) to full tint (1% transmittance) state, depending on incident solar radiation and outdoor temperature. The fac¸ade of Room A on the right side is a low-emittance double glazing with 62% visi-ble light transmittance, as a reference condition. The modelled scene of each office is illustrated in Figure 2 b).

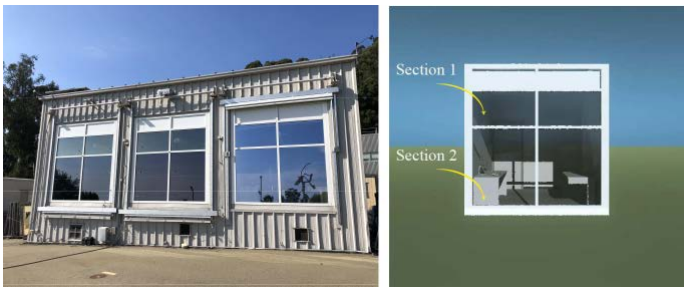

(a) Daylighting testbed (b) Modelled scene

Fig. 2. A daylighting testbed with three parallel offices

In the prototyping phase, the EPD was placed outdoors in front of the EC fac¸ade (0.5 m distance to the fac¸ade, 1.5 m above the ground) with its axis of lens in the orthogonal plane of the fac¸ade for experimental convenience, as shown in Figure 3 a),

instead of attaching the EPD to the glass as designed. It is assumed that the position translation of the imaging system has negligible influence on the lighting simulation. The EPD, as a controller, was connected to the EC glazing driver to pro-vide tint state signal, according to optimization results. The optimized tint states were determined according to the real-time lighting simulation results based on the monitored lumi-nance distribution of the sky (and landscape) performed by the EPD. In each room interior, lux-meters (LiCor LI-210SA, ±3% of reading,) and cameras (Canon EOS 5D) were positioned to measure WPI and monitor discomfort glare as references, for the purposes of cross validation and assessment of control per-formance. The digital single-lens reflex (DSLR) camera, em-ploying HDR imaging techniques, composites multiple low dy-namic range images into an HDR image. The HDR image, cali-brated by the vertical illuminance measured by an adjacent ver-tical sensor, is used to calculate glare risk metrics, including daylight glare probability (DGP), using the evalglare program in RADIANCE software [46] from the captured view point.

(a) EC glazing with EPD controller (Prototyping)

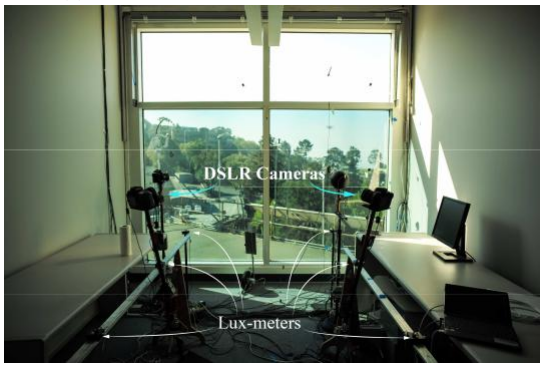

(b) Lux-meters and cameras offering reference measurement

(Validation) Fig. 3. Experimental set-up

3.2. Simulation method

In this paper, WPI and DGP are two metrics that are used to evaluate visual satisfaction of occupants in the EC glazing control. Although quasi real-time lighting simulation results can be achieved using the backward ray-tracing algorithms [47], the iterative computation of these algorithms is time-consuming to assess lighting conditions for various tint state combinations of EC glazing, especially on a compact platform. Therefore, a matrix algebraic approach [48, 49] of lighting simulation is employed on the EPD in order to make iterative calculation more time-efficient. The idea is to employ the RADIANCE software [46] to pre-compute a set of matrices that relate the sky luminance distribution to the contributed WPI in building interior. Instead of using the original five-phase method developed for sky luminance models [49], the matrix algebraic approach is modified for split-pane EC glazing control based on high-resolution monitoring of the sky luminance distribution as shown in Equation (1), where numeric subscripts 1 and 2 denote the independent contribution of the upper daylight window sec-tion and that of the lower view window section respectively, as illustrated in Figure 2 b). Equation (1) calculates the horizontal illuminance vector of work-plane $\mathbf{i_{wp}}$, in which the mean is re-garded as WPI in EC glazing control. Equation (1) separates the contribution from the sky vault and the sun, due to the required different resolution.

$$\mathbf{i_{wp}} = \mathbf{V_1}\,\mathbf{TD_1}\,\mathbf{s} + \mathbf{C}_{d\,s1}\mathbf{s}_{sun} + \mathbf{V_2}\,\mathbf{TD_2}\,\mathbf{s} + \mathbf{C}_{d\,s2}\mathbf{s}_{sun} \quad (1)$$

- $\mathbf{C}_{d\,s1}$ is the solar coefficient matrix for the upper daylight window section, which is associated with the contribution from the sun luminance to the horizontal illuminances at corresponding positions on the work-plane through the upper daylight window section
- $\mathbf{C}_{d\,s2}$ is the solar coefficient matrix for the lower view win-dow section, which is associated with the contribution from the sun luminance to the horizontal illuminances at corresponding positions on the work-plane through the lower view window section
- $\mathbf{D_1}$ is the daylight matrix for the upper daylight window section, which relates the luminance of each sky patch to an incident direction on the front EC glazing plane of the upper daylight section
- $\mathbf{D_2}$ is the daylight matrix for the lower view window sec-tion, which relates the luminance of each sky patch to an incident direction on the front EC glazing plane of the lower view section
- $\mathbf{i_{wp}}$ is a vector containing the computed illuminance at defined position on the work-plane in the testbed
- $\mathbf{s}$ is the sky vector, each element of which contains the lu-minance value from a sky patch, excluding the sun com-ponent
- $\mathbf{s}_{sun}$ is the direct sun vector, a sparse vector containing only the luminance of the sun component with an apex angle of 0.53°
- $\mathbf{T}$ is the transmission matrix (BTDF) of the EC glazing, which relates light flux transfer from each incident direc-tion on the front glazing plane to an emergent direction on the glazing interior plane
- $\mathbf{V_1}$ is the view matrix for the upper daylight window sec-tion, which is associated with the contribution from each

emergent direction from the upper daylight window section (interior plane) to the light horizontal illuminances at corresponding positions on the work-plane

- **V2** is the view matrix for the lower view window section, which is associated with the light contribution from each emergent direction from the lower view window section (interior plane) to the horizontal illuminances at corresponding positions on the work-plane

The product of **V**, **T**, **D**, **and s** calculates the work-plane illuminance contributed by the sky vault and landscape, while product of $\mathbf{C}_{d\,s}\,\mathbf{s}_{sun}$ computes the illuminance contributed by the sun, through the upper daylight window section or through the lower view window section. Noticeable error in illuminance calculation using the five-phase matrix algebraic approach has been reported by Lee et al. [50], which is due to the resolu-tion mismatch between the transmission matrix **T** (commonly 10 − 15° resolution) and the sun orb which only spans an apex angle of 0.53°. In order to reduce the simulation error and to re-solve the veiling glare due to secondary reflection on specular surfaces from the surrounding environment, matrices in Equa-tion (1) employ a high resolution angular basis, based on the subdivided Tregenza angular basis [51], instead of the com-monly used Klems angular basis (10 − 15° resolution) [52]. In Equation (1), each element of the sky vector **s** (Reinhart MF:5, 3602 elements or directions) spans an apex angle of 2.4°, and each incident and emergent direction in transmission ma-trix T (Reinhart MF:4, 2305 × 2305) subtends an apex angle of 3°. Therefore, after generating the luminance map of the sky and landscape with 1.2 million patches on the EPD, the solar component is extracted from the luminance map and it is sub-sampled with 3602 elements to generate a sky vector **s** after being pre-filtered. The sun position is discretized into 5176 lo-cations (Reinhart MF:5) in $\mathbf{s}_{sun}$, each spanning an apex angle of 0.53°, and the sun is approximated to the nearest location with a maximal 1.5° bias. Although preparation of these matrices is relatively time consuming, the iterative calculation of work-plane illuminance $\mathbf{i_{wp}}$ (performed on the EPD) only involves matrix multiplication, which is substantially more time-efficient than the ray-tracing approach. To generate view images (reso-lution 500 × 500) for DGP calculation, the routine is similar to that of the work-plane illuminance vector $\mathbf{i_{wp}}$ in Equation (1); the only differences are matrices **V** and $\mathbf{C}_{d\,s}$ that are changed into arrays of view images.

The bi-directional transmittance distribution function (BTDF) is employed in the lighting simulation as the matrix T in Equa-tion (1). BTDF, which characterizes light transmission behavior of a complex fenestration system (CFS), is defined as the ratio of emergent luminance to incident illuminance on the incident plane [53]. BTDF has been commonly used to represent a CFS in lighting simulation without knowledge of material property or geometry of a CFS. which speeds up computation. In this paper, the 'genBSDF' program in RADIANCE software was employed to generate the BTDF data of the EC glazing at dif-ferent tint states. The original genBSDF program was modified to output BTDF data based on the Tregenza angular basis sub-divided by a factor of four (Reinhart MF:4, 2305 × 2305) in-stead of the default Klems angular basis (145 ×145), to resolve small-scale glare source in lighting simulation. Figure 4 illus-trates the tone-mapped HDR image of the BTDF matrix of EC glazing at 18% transmittance, which is essentially a diagonal matrix (black region denotes zero).

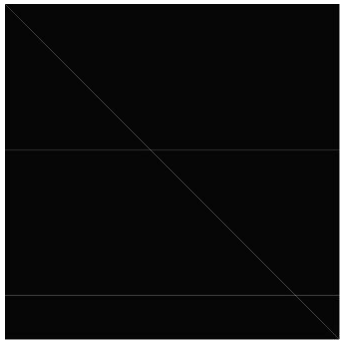

Fig. 4. Tone mapped image of the BTDF matrix of EC glazing at 18% transmittance

3.3. Control logics

EC glazing tint control is an optimization process to ensure vi-sual comfort for occupants, satisfy minimum daylight provi-sion requirements defined by EN12464-1, and maximize oc-cupants' view quality outwards through fac¸ades, according to Equation (2). The work-plane is defined as a 1.3×1.5 m^2 rectan-gle at the height of 0.8 m above the floor in the center of the of-fice, as a virtual desk enclosed by the six lux-meters as shown in Figure 3 b). The horizontal illuminances at the same positions of lux-meters (at 0.75 m, 1.5 m, 2.25 m distance to the fac¸ade) are simulated by the EPD based on a monitored luminance map of the sky, the mean of which is regarded to be WPI. The WPI is constrained to be greater than 500 lux, which satisfies minimal daylight provision requirement (En 12464-1 [9]), and to be be-low 2000 lux, which mitigates excessive daylight provision and solar heat gain. Although there is no consensus on the upper limit of WPI, the upper bound between 2000 lux and 3000 lux has been used in studies of shading control [54] and daylight-ing analysis [55, 56], exceeding which is associated with vi-sual and thermal discomfort. In this study, the WPI range [500, 2000] lux is adopted to demonstrate the daylighting control per-formance, which can also be modified accordingly in a specific application to meet users' lighting preference. Two view per-spectives are defined at the mid-point of two parallel edges of the virtual desk at the height of 1.2 m, orienting 45° and 135° re-spectively, towards the fac¸ade with a 10° elevation angle, which makes both the window and sunlit area on the wall to be in the center of FOV, as the direction of camera lens shown in Figure 3 b). The defined view directions emulate two occupants sitting on two sides of the virtual desk and facing the fac¸ade as one of the worst cases regarding sensing discomfort glare, since major potential glare sources (light transmitted through the window or reflected from the wall) are in the FOV of occupants. The higher DGP from the left (DGP_l) or right (DGP_r) perspective

is constrained below 0.35 by the EPD controller, which lim-its the discomfort glare within the imperceptible level for both view directions. When the EC glazing approaches a lower lumi-nous transmittance state, the outside view becomes darker and is tinted with a blueish color shift. To optimize the view qual-ity for occupants, the cost function is established to maximize transmittance of the lower view window section β_2 [40], pro-vided that the constraint is satisfied with regard to the daylight provision (WPI) and discomfort glare (DGP).

Maximize:

$$\beta_2 \tag{2a}$$

Subject to:

$$500 \text{ lux} < \text{WPI} < 2000 \text{ lux} \tag{2b}$$

$$\text{DGP} = \sup\{\text{DGP}_l, \text{DGP}_r\} < 0.35 \tag{2c}$$

Figure 5 illustrates a flowchart of EPD evaluation in tuning tint states of the split-pane EC glazing to optimize daylighting for occupants' visual satisfaction. The time consumption required for each stage is labelled next to the corresponding diagram block. The EPD starts with monitoring the luminance distri-bution of the sky vault and ground fraction facing the fac¸ade, including that of the sun, clouds, the sky vault, and landscape.

A high-resolution luminance map is generated and is then trans-formed into a sky vector **s** with 3602 elements and a direct sun vector $\mathbf{s}_{sun}$ with solar luminance in one of its 5176 elements, as defined in Equation (1). Following matrix multiplication in Equation (1), the WPI is calculated for 16 EC tint combinations, with four tint states of the upper daylight window section and four states of the lower view window section, the computation of which is accomplished in 10 ~ 20 s. The EC tint combina-tions with corresponding WPI within the constraint are selected for further assessment of discomfort glare. If no combination satisfies the WPI range, this suggests the WPI is below 500 lux for all tint combinations and the optimal tint states should be clear (60% transmittance) for both EC glazing sections to ad-mit a maximal daylight flux, since it is impossible for WPI to exceed 2000 lux when both glass sections are at 1% transmit-tance. Next, the HDR view images are generated for selected tint combinations, which requires 400 ~ 500 s, and then the corresponding DGP is calculated from left and right view per-spectives. The optimal tint combination is the one that satisfies its DGP below the perceptible glare threshold, with the clear-est possible tint in the lower view window section to secure outwards view quality. Finally, the EPD sends a control sig-nal of the determined tint combination to the EC glazing driver to adjust the daylighting in buildings. Although one evaluation of control algorithms requires 8-10 min, this paper employs an interval of 15 min with additional time margin to synchronize with reference apparatuses for comparison.

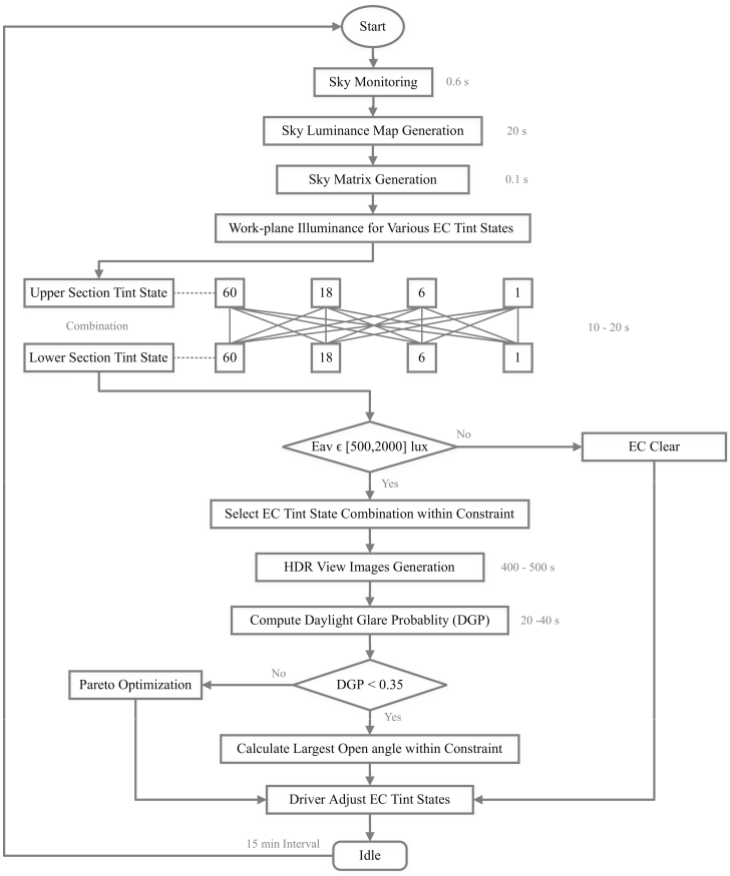

Fig. 5. Flowchart of each EPD evaluation in EC glazing control

In order to outline the performance, regulated daylighting con-dition in Room C, with its EC glazing control performed by the EPD, was compared with that in Room A and B, as illustrated in Figure 6. The interior set-ups are the same for the three rooms with identically positioned lux-meters and reference cameras; the only difference is the window glazing states. The EC glaz-ing of Room B is controlled based on the weather data (direct normal and diffuse horizontal irradiance) at LBNL and Perez all-weather model [57] as input to the same matrix algebraic approach introduced in Section 3.2, as a conventional control case. With a low-emittance glazing, Room A acts as a reference case illustrating a daylit environment without dynamic control.

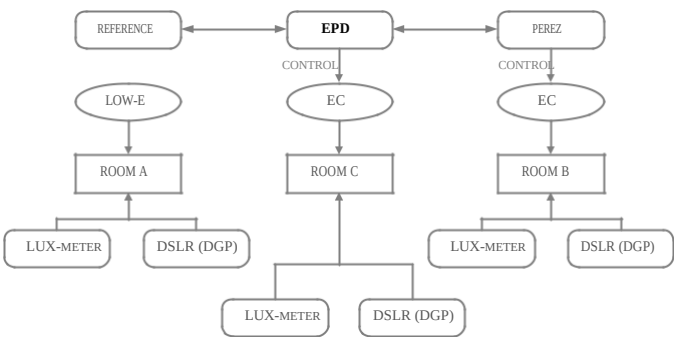

Fig. 6. Parallel experiments assessing EC glazing control

4. Empirical validation

4.1. Cross comparison

Although the EPD was demonstrated in its capability of real-time lighting simulation of work-plane illuminance by Wu et al. [41, 45] in several studies, a cross comparison experiment was conducted to further assess the performance of EPD in WPI, image rendering, and DGP calculation in the testbed with static tinted EC glazing.

The experiment was implemented under a clear sky on Sept. 21st, 2018. The EC fac¸ade was tinted at 18% transmittance (light tint) for both the upper daylight and lower view window sections throughout the day. The EPD was positioned in front of the testbed to monitor luminance distribution of the sky and to perform a lighting simulation in WPI and DGP every 15 min from morning to evening at the defined interior positions as described in Section 3.3. As a reference, lux-meters were used to monitor the WPI every minute and cameras recorded HDR view images at five min intervals, based on which reference DGP was computed. Figure 7 shows the WPI and DGP in sub-figures a) and b) respectively, where green curves denote sim-ulated value performed by the EPD, and grey curves represent the measured values from reference apparatuses. The density of data points on the green and grey curves are different, since the EPD performed the lighting simulation at a lower frequency as compared to the sampling frequency of the reference lux-meters and cameras. The average root-mean-square error (RMSE) of the simulated WPI is 17.6% and that of DGP is 2.7%, as com-pared to reference values.

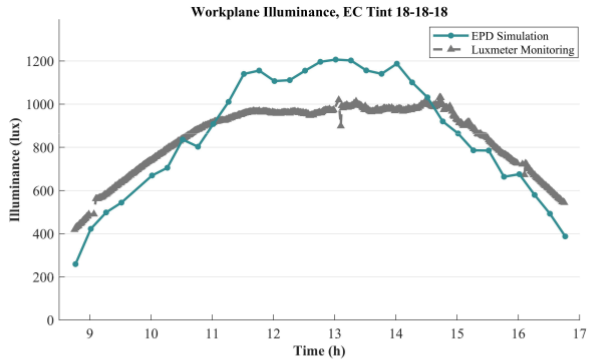

(a) Workplane illuminance (WPI)

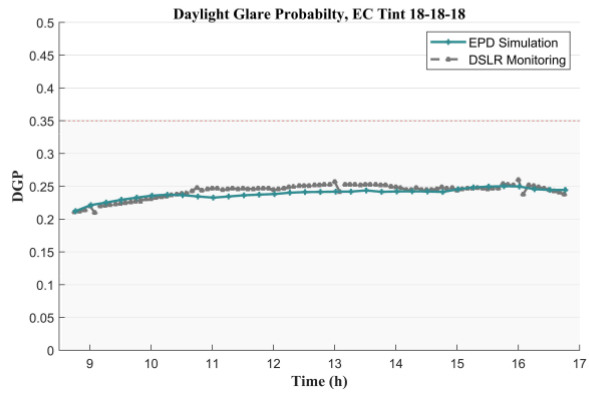

(b) Daylight glare probability (DGP)

Fig. 7. WPI and DGP with EC glazing at 18% transmittance

In a second comparison, the upper daylight glazing section was set to 1% transmittance and the lower view glazing section was set to 6% transmittance. Figure 8 shows a rendered view image performed on the EPD and an image captured by the camera on the right side in the testbed respectively at the same time from identical view perspectives. A sound correspondence on the light and shadow on the wall can be found between the two sub-figures. Although the landscape of sub-figure a) has a mo-saic pattern due to the sub-sampling process in generating the sky vector, the landscape profile is discernible and match the captured HDR view image as shown in sub-figure b).

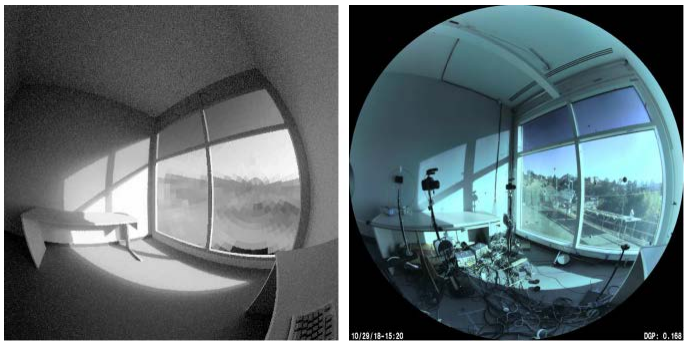

(a) Simulated by EPD (b) Captured by camera

Fig. 8. View images with EC glazing at 1% (upper) and 6% (lower) transmittance

4.2. EC glazing control

For EC glazing control, the EPD monitored luminance distribution of the sky (and landscape), simulated interior WPI and DGP at defined positions, and optimized tint states for EC glazing, following the flowchart in Figure 5. The EPD performed the evaluation and controlled EC tint combination of Room C every 15 min, as described in Section 3.3. To outline the performance of EPD, weather data (direct normal and diffuse horizontal irradiance) from a weather station at LBNL was used with the same lighting simulation method (matrix algebraic approach) employing the Perez all-weather model, as described in Section 3.2, to control the EC glazing simultaneously in Room B, as a conventional control strategy based on weather data. Room A provided an unregulated daylighting condition with fixed glazing transmittance (low-emittance window) as reference. To simultaneously evaluate the glazing control performance in the three parallel rooms, lux-meters and cameras were used to monitor WPI and DGP respectively. Experiments were conducted from Oct. 22nd to 28th, 2018 under various sky conditions, including clear, clear with thin clouds, and partly cloudy.

Figure 9 shows the result of WPI on Oct. 24th under a clear sky. Sub-figure a) shows the mean horizontal illuminance on workplane monitored by six lux-meters as WPI in Room C with its EC glazing controlled by EPD, denoted by green curves in the upper section of Figure 9 a). The grey curve represents the WPI monitored by lux-meters in Room A without daylighting regulation as a reference (low-emittance window). The lower section in Figure 9 a) illustrates the optimized tint states for EC glazing in the upper daylight section and lower view section. Before the EPD started the first evaluation, WPI had exceeded the upper constraint bound (2000 lux). Therefore, the controller switched the EC glazing to 1% transmittance in the upper section and to 18% in the lower section from the initial clear tint state (60% transmittance). The WPI dropped accordingly into the constraint (500~2000 lux, the highlighted region), in which the computation time of EPD and the response time of EC glaz-ing (10~30 min) contributed to the delay. When the sky lumi-nance surged at 10:40, the EPD further tinted the lower window section to 6%, which suppressed the increased WPI below 2000 lux. Throughout the day, the WPI was maintained within the constraint, as the glazing tint states were optimized dynamically according to variation in the luminance distribution of the sky. In the evening, when the WPI approached the lower bound (500 lux), the EC glazing was bleached to allow in sufficient day-light. Figure 9 b) illustrates the daylighting performance with the EC glazing control in Room B based on real-time weather data (of direct normal and diffuse horizontal irradiance) and the Perez all-weather model as a conventional control strategy. The green curve in the upper section of the figure denotes the WPI monitored by lux-meters in Room B with its EC glazing con-trol based on sky model, while the grey curve represents the same WPI monitored in Room A without daylighting control as a reference. Due to the limited accuracy of real-time lighting simulation based on weather data and the Perez sky model [41], the regulated WPI shows a higher frequency of exceeding the upper limit compared with that controlled by the EPD. The time fraction that WPI lies in constraint is 83% for the EC glazing control based on the EPD in Room C, while it is 41.2% for the EC glazing control based on weather data and Perez all-weather model in Room B, as compared with 9.0% without daylighting control in Room A, under a clear sky.

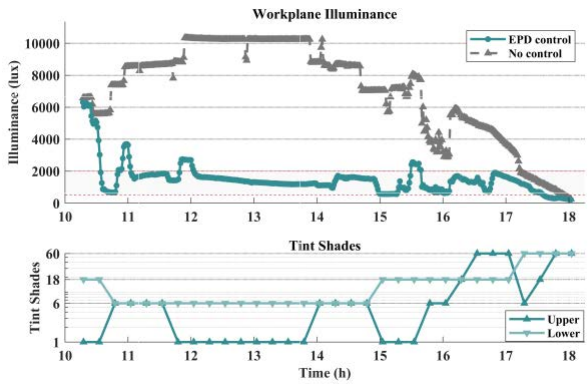

(a) Control based on EPD

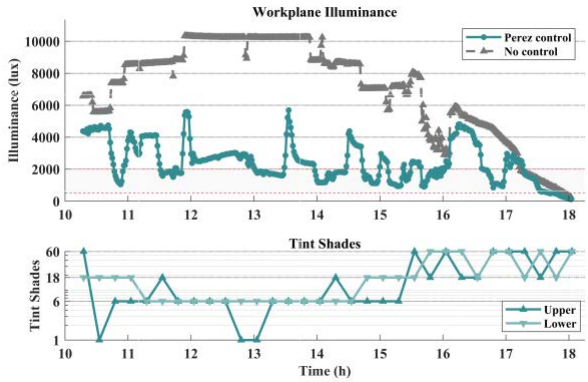

(b) Control based on weather data and Perez sky model

Fig. 9. WPI with EC glazing controlled by different methods (clear sky)

Figure 10 a) shows the maximum DGP monitored by the two cameras in room C with EC glazing controlled by the EPD (green curve) on the same day, as compared with that in room

A without dynamic EC glazing (grey curve). Since cameras recorded DGP at a five min interval, the data points are sparser than those in Figure 9. The DGP was mitigated from above intolerable (> 0.45) to imperceptible level (< 0.35) after EPD started to operate. Although the DGP in room A without EC glazing protection exceeded the comfort zone, the DGP in room C with automated EC glazing tints based on EPD control was maintained in the imperceptible glare range, except when it reached a perceptible level ([0.35, 0.4]) at 15:10 when the sun was in the FOV of the left camera through the upper window section. Even though the upper daylight window section was tinted to the full tint state (1% transmittance), the DGP still slightly exceeded the imperceptible bound due to the intensive luminance of the sun orb, which is one limitation of mitigat-ing disability glare due to the sun using EC glazing. Figure 10

b) presents the DGP monitored by cameras in room B with EC control based on real-time weather data and the Perez all-weather model (green curve). The curve shows a relatively high chance of exceeding the comfort range and the frequency of variation in tint states is increased. The time fraction that DGP was maintained within comfort constraint is 94.6% for the EC glazing control based on the EPD in Room C, while it is 61.2% for the EC glazing control based on weather data and Perez all-weather model in Room B, as compared to 7.5% without daylighting control in Room A, under a clear sky.

Under a clear sky with thin clouds, the motion of clouds con-tributed to the fluctuation of daylight provision in the building interior on Oct. 27th, as the WPI illustrated in Figure 11. Sub-figure a) shows the WPI monitored by lux-meters in Room C with EC glazing controlled by the EPD (green curve), com-pared with that in Room A with a static low-emission window (grey curve). Although the external daylight condition varied throughout day, the WPI tuned by EC glazing controlled by the EPD was maintained within the [500, 2000] lux range 70.3% of the work time, as compared to 9.7% of the time without EC glazing protection. The rapid movement of clouds and re-sponse delay of both the EPD and EC glazing contributed to the over-suppression of WPI below 500 lux at 15:00. Sub-figure b) presents the WPI monitored by lux-meters in Room B with EC glazing control based on real-time weather data and the Perez all-weather model (green curve). Since a sky model does not resolve cloud pattern distribution in real-time, the day-light provision cannot be simulated accurately based on an as-sumed smooth sky luminance distribution by the sky model, and the WPI exceeded the upper bound of 2000 lux multiple times, which was possibly a result of underestimated WPI sim-ulation, with 25.8% of the time within constraint. Moreover, EC tint states controlled by the EPD showed a relatively better stability with less variations than those of EC glazing control based on weather data and sky model.

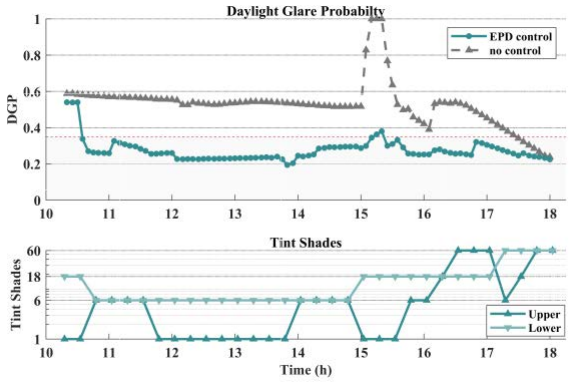

(a) Control based on EPD

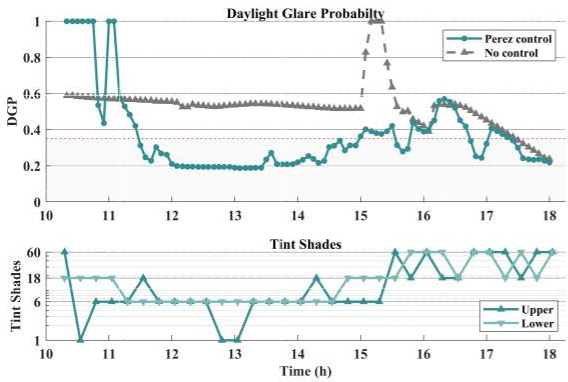

(b) Control based on weather data and Perez sky model

Fig. 10. DGP with EC glazing controlled by different methods (clear sky)

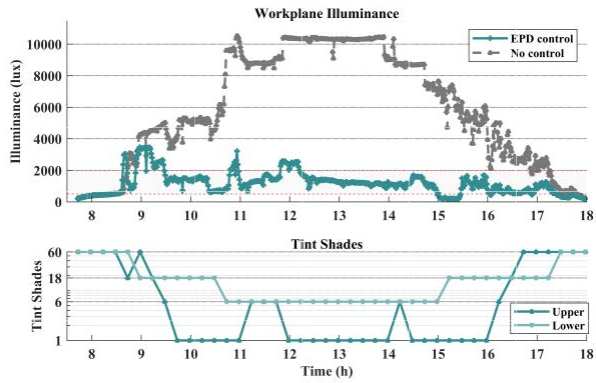

(a) Control based on EPD

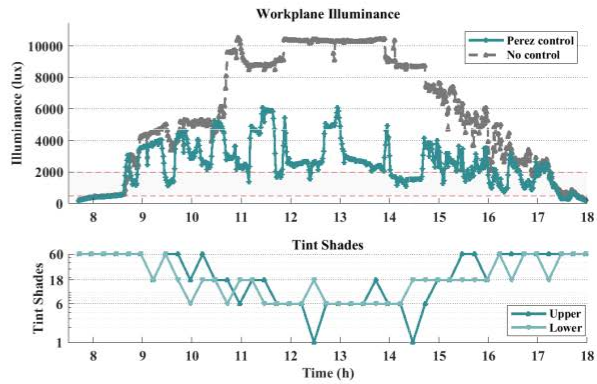

(b) Control based on weather data and Perez sky model

Fig. 11. WPI with EC glazing controlled by different methods (thin clouds)

Figure 12 a) shows the DGP monitored by cameras in Room C with EC glazing controlled by the EPD (green curve), as compared with that monitored by cameras in Room A without daylighting control (grey curve). The DGP fluctuated throughout the day due to the movement of thin clouds, occluding the sun occasionally. The time ratio of DGP within the imperceptible range reached 93.5% with EC glazing controlled by the EPD, while it reached 35.8% with EC glazing control based on weather data and a sky luminance model as shown in Figure 12 b), as compared to 22.8% without EC glazing protection. The EC glazing control based on the EPD showed a pronounced advantage over the control based on weather data in regulating daylight provision and tempering discomfort glare under a clear sky with thin clouds.

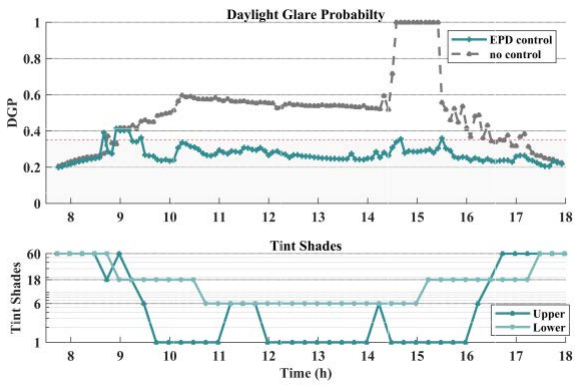

(a) Control based on EPD

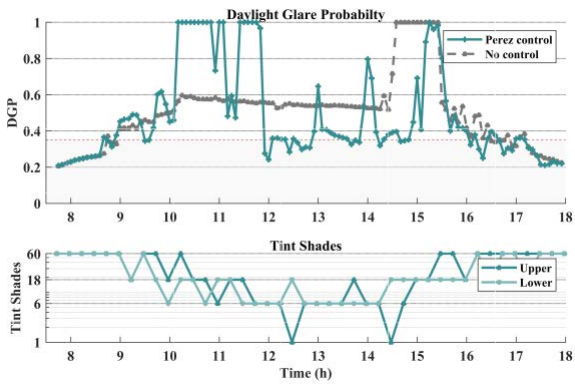

(b) Control based on weather data and Perez sky model

Fig. 12. DGP with EC glazing controlled by different methods (thin clouds)

Partly cloudy skies are the most challenging sky conditions for the EC glazing control, since daylight availability varies drastically in both magnitude and frequency due to movement of thick clouds, when the performance of EPD can be limited by its computational time consumption and delay of EC window response. Figure 13 presents the WPI recorded by lux-meters in room C with the EC window controlled by the EPD (green curve) on Oct. 23rd under a partly cloudy sky, as compared to that in Room A with a low-emission window (grey curve). When the EPD started to operate and sent a signal to modify EC tint states, the external daylight decreased sharply in intensity and the WPI was over-suppressed marginally below 500 lux at 11:00 due to the delay of EPD evaluation and EC glazing response. The tint states of EC window at 11:00 were optimized for the daylight condition 20 min before. The overshoot or over-suppression of WPI was also due to the response delay at 11:30, 12:10, 13:30, 13:50, 15:10, and 15:30. Although the rapid motion of clouds deteriorated EPD performance, the EPD outperformed the weather data and sky luminance model based con-trol in maintaining WPI as shown in Figure 13 b) (green curve), with 63.3% of the time within constraint rather than 49.1% of the time based on weather data and a sky model, compared with 9.1% of the time in constraint without daylighting control.

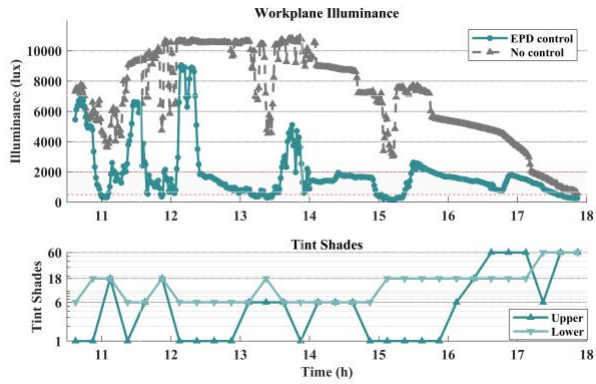

(a) Control based on EPD

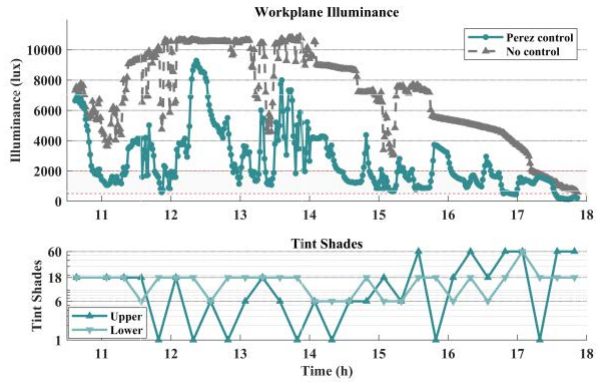

(b) Control based on weather data and Perez sky model

Fig. 13. WPI with EC glazing controlled by different methods (partly cloudy)

The DGP, monitored by cameras in Room C with EC glazing controlled by the EPD, also fluctuated under the partly cloudy sky, as shown in Figure 14 a) (green curve). With daylighting controlled by the optimized EC tint states using the EPD, the time fraction of DGP within imperceptible level reached 88.5% of the time, while it reached 63.2% of the work time with EC glazing control based on weather data and a sky model as shown in 14 b), compared with 6.8% of the time in room A with a low-emission coated glazing.

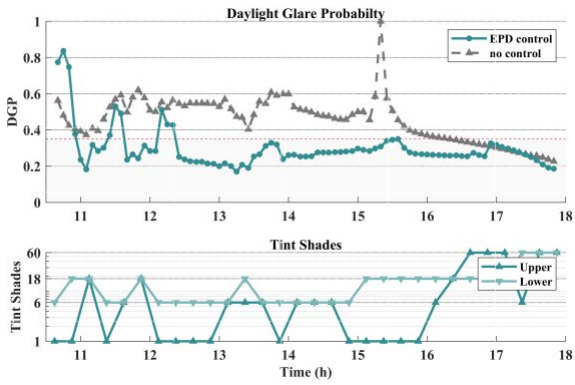

(a) Control based on EPD

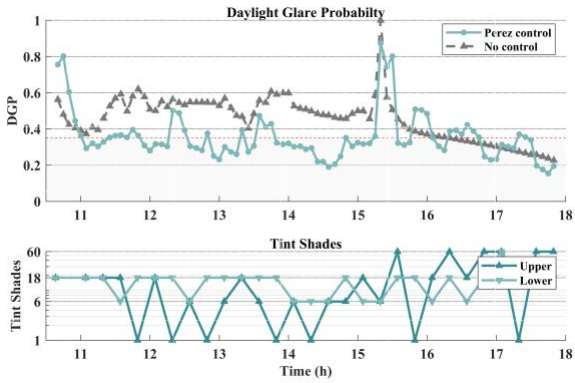

(b) Control based on weather data and Perez sky model

Fig. 14. DGP with EC glazing controlled by different methods (partly cloudy)

Table 1 summarizes the time fraction that WPI and DGP were maintained within constraint with the window facadescontrolled by different strategies under various sky conditions for the vi-sual satisfaction of occupants. It can be observed that EPD con-trol achieved the highest ratio of daylight provision (83% on av-erage) and glare risk (95% on average) within constraint range under clear skies when the external daylight condition changed slowly. The EPD controlled EC glazing (68% for WPI, 94% for DGP on average) showed pronounced superiority as com-pared with EC glazing control based on weather data and the Perez all-weather model (28% for WPI, 41% for DGP on aver-age) under clear skies with thin clouds, since the EPD based on sky luminance monitoring was able to resolve the varying cloud patterns achieving enhanced accuracy of real-time daylighting simulation. Although the EPD was limited by its computation time and delay of EC glazing response under partly cloudy skies with rapid motion of clouds, it was able to dampen the variation of daylight provision and glare risk for occupants. Its perfor-mance can be improved by reducing the computation time via advanced hardware or simplified algorithms, and by employing the new EC glazing technology with fast transition.

Table 1: Ratio of time regarding WPI and DGP within constraints

Date	Sky type	WPI			DGP			Total time
		EPD	Perez	No control	EPD	Perez	No control	(min)
10/22	Clear Sky	84.5%	53.8%	9.0%	98.7%	81.3%	6.7%	435
10/24	Clear Sky	83%	41.2%	9.0%	94.6%	61.2%	7.5%	465
10/25	Clear Sky	80.5%	36.2%	6.6%	93.1%	63.2%	3.4%	435
10/26	Clear/thin clouds	66.1%	29.4%	6.9%	95.4%	47.1%	9.2%	435
10/27	Clear/thin clouds	70.3%	25.8%	9.7%	93.5%	35.8%	22.8%	615
10/23	Partly Cloudy	63.3%	49.1%	9.1%	88.5%	63.2%	6.8%	435
10/28	Partly cloudy	61.2%	42.3%	15.9%	81.8%	40.5%	28.6%	630

Note: the constraint of WPI is [500, 2000] lux, that of DGP is ≤ 0.35, according to Equation (2)

5. Discussion

In this paper, the EPD performance of the DGP simulation was compared with DSLR cameras based on captured HDR im-ages in Section 4.1. Although DSLR cameras with high-quality fish-eye lens have been widely used by researchers to quan-tify discomfort glare, cameras commonly require a relatively long exposure time (commonly approximately 30 s) to achieve a wide luminance detection range and a low-transmittance neu-tral density (ND) filter to attenuate solar luminance due to its limitation of shutter speed when the sun is in FOV. Researchers also depend on the linear transformation of color space to gen-erate luminance values from captured images, the spectral re-sponse mismatch with the photopic luminosity function V(λ) being commonly unidentified. With spectral correction by opti-cal filters, the EPD has a close spectral response to the V(λ) (f_1' = 8.89%) in monitoring sky luminance distribution. Its high-speed shutter makes the acquisition time relatively short (in 1.3 s), with a dynamic range of 150 dB for luminance de-tection, which is advantageous in capturing fast-moving clouds regarding effects of motion blur. Moreover, a single EPD is able to simulate DGP values at multiple defined positions and view directions simultaneously, while multiple cameras must be used to accomplish the task using captured images despite their ac-tual positions. In EC glazing or shading control, it is impractical to place multiple DSLR cameras at occupants' view positions, due to privacy issues and occupants' random motions occluding the FOV of DSLR cameras.

In EC window control, the EPD operates at 15 min intervals to modify tint states of EC glazing continually according to dy-namic sky conditions. When the sky varies more rapidly than the evaluation frequency of EPD, the EPD can miss the instan-taneous variation of the sky, or the delayed response of EPD together with that of the EC glazing can contribute to overshoot-ing or over-suppression of WPI and DGP. Figure 15, captured by one DSLR camera in Room A, illustrates the overshooting of WPI at local time (LT) 12:10 in Figure 13 on Oct. 23rd under a partly cloudy sky. As highlighted in Figure 15 a), a cloud was on the right side of the window, 2 min before the EPD eval-uation at LT 11:52. After evaluation (3 min later), the cloud moved to the left side of the window, as highlighted in Fig-ure 15 b). In fact, the cloud occluded the sun when EPD eval-uated the sky conditions at LT 11:52. Therefore, the resulting low daylight availability, at that moment, caused the EPD to in-crease the transmittance of the EC window to 18% for both win-dow sections. After 15 min, when the tint states reached 18% transmittance and the cloud moved away, the excessive day-light injection contributed to the overshoot of WPI at LT 12:10 in Figure 13. To resolve the uncommonly fast moving clouds, advanced hardware can be applied to enhance the computation speed of EPD if the increased cost is acceptable to users. Al-ternatively, employing simplified algorithms can also increase evaluation frequency of the EPD despite sacrificing simulation accuracy.

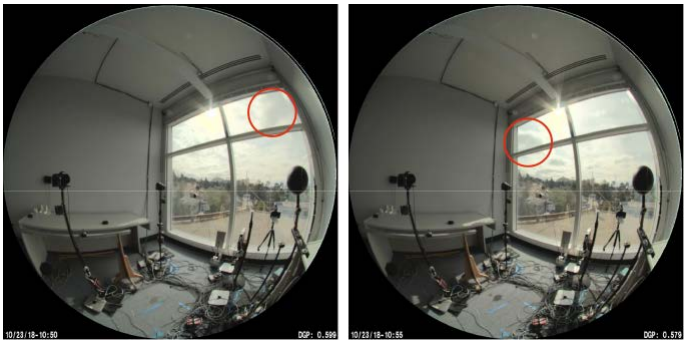

(a) Before an evalutation (LT 11:50) (b) After an evalutation (LT 11:55)

Fig. 15. Rapid motion of clouds (captured in Room A)

The solar elevation angle during the experimental period (Oct. 22nd to 28th, 2018) was approximately 40° at noon, between that of the autumn equinox (52°) and winter solstice (30°). The sun was in the FOV from the right view perspective through the upper window section, as illustrated by Figure 15. This period offered the condition to investigate the EC glazing control in mitigating discomfort glare from the sun. In summer, less dis-comfort glare is expected since the solar elevation angle (75°) is higher at noon and the sun can be occluded by the ceiling for occupants. At winter solstice, the sun is visible through the upper window section, which is similar to the experimen-tal period, however, the 10° difference in elevation angle can possibly influence the level of discomfort glare. Although vari-ous sky conditions have been assessed including clear sky, clear sky with thin clouds, and partly cloudy sky during the limited period, the influence of the solar elevation angle on the con-

trol performance of the EC glazing will be investigated during different seasons in the future.

6. Conclusion

The integration of electrochromic (EC) glazing with an efficient tint control system is a major challenge for the broad applica-tion of EC glazing. This paper presents a highly integrated de-sign of a stand-alone EC glazing control system to achieve vi-sual comfort for occupants. An embedded photometric device (EPD), which acts both as the sensing unit and the controller, can monitor the luminance distribution of the sky and landscape and perform real-time lighting simulation of a building interior. Based on simulated results, tint states of a split-pane EC glaz-ing are optimized to maintain work-plane illuminance and to mitigate discomfort glare for occupants, which potentially mit-igates excessive solar heat gain.

A cross comparison was performed to demonstrate the lighting simulation capability of EPD in work-plane illuminance (WPI), image rendering, and daylight glare probability (DGP) calcula-tion, with lux-meters and calibrated cameras. Based on a matrix algebraic approach, the EPD was able to assess WPI and DGP in the building interior for 16 tint combinations of a split-pane EC window and to optimize EC glazing tint to achieve visual comfort within 8-10 min. 'In-situ' experiments of split-pane EC glazing control were conducted in a daylighting testbed un-der various sky conditions. Three parallel office rooms illus-trated daylighting conditions controlled by EC window with the EPD control, with the conventional control based on real-time weather data and sky luminance model, and without daylighting control (clear glazing) respectively. The results showed that the WPI was within the confined range (WPI∈[500, 2000] lux) 83% of the working time and the DGP within comfort range (DGP ≤ 0.35) 95% of the time fraction with daylighting controlled by the automated EC glazing based on the EPD under clear skies; under clear skies with thin clouds, the WPI was within confined range during 68% of the time and the DGP during 94% of the time. Although the computation time of EPD and response de-lay of EC glazing limited the performance of daylighting con-trol under partly cloudy skies, the EPD controlled EC glazing was able to dampen the WPI and DGP variation when daylight condition varied rapidly, with 62% and 85% of the time main-tained in the confined range respectively. The split-pane EC window glazing controlled by the EPD was superior at reach-ing visual comfort as compared to a conventional strategy with EC glazing control based on weather data and sky luminance models.

Furthermore, the designed EC control system also features mer-its in installation convenience, since the integrated design avoids placing separate sensors and avoids wiring issues in the build-ing interior. As a decentralized system, the designed EC con-trol system is independent of weather data or weather stations which commonly require the access to a non-shadowing roof. Additionally, pre-knowledge of window position and direction is not required since a relative coordinate is established in the EPD controller. Moreover, the glare due to secondary reflection on specular surfaces from surroundings can be mitigated poten-tially, since the EPD monitors the luminance distribution of the exterior space.

Investigation on the application of the integrated EC control system in open-planned offices will be conducted, and exper-iments of EC glazing control will be extended to different sea-sons to assess the influence of the solar elevation angles in the future. To cope with the rapid variation of daylight under partly cloudy skies, improvement in the response delay of EPD will be studied by employing simplified algorithms and advanced com-putation hardware and in using faster responding EC glazing.

7. Acknowledgement

The author would like to acknowledge the technical support of Mr. Pierre Loesch from EPFL, Switzerland and Mr. Christoph Gehbauer from LBNL, USA. This research project was finan-cially supported by the Swiss Innovation Agency Innosuisse (CTI.2014.0119) and by the Zeno Karl Schindler Foundation and is part of the Swiss Competence Center for Energy Re-search (SCCER FEEB&D). This work was also supported by the Assistant Secretary for Energy Efficiency and Renewable Energy, Building Technologies Program, of the U.S. Depart-ment of Energy, under Contract No. DE-AC02-05CH11231 and the California Energy Commission through its Electric Pro-gram Investment Charge (EPIC) Program on behalf of the citi-zens of California.

References

[1] Ø. Aschehoug, Daylight in glazed spaces: Daylight conditions in long glazed streets examined with physical models in an artificial sky and com-puter calculations, Building research and information 20 (4) (1992) 242– 245.

[2] A. S. Bahaj, P. A. James, M. F. Jentsch, Potential of emerg-ing glazing technologies for highly glazed buildings in hot arid climates, Energy and Buildings 40 (5) (2008) 720 – 731. doi:https://doi.org/10.1016/j.enbuild.2007.05.006.

[3] X. Wang, C. Kendrick, R. Ogden, N. Walliman, B. Baiche, A case study on energy consumption and overheating for a uk industrial building with rooflights, Applied energy 104 (2013) 337–344.

[4] A. Tzempelikos, A. K. Athienitis, The impact of shad-ing design and control on building cooling and light-ing demand, Solar Energy 81 (3) (2007) 369 – 382. doi:https://doi.org/10.1016/j.solener.2006.06.015.

[5] F. Beute, Y. A. de Kort, Salutogenic effects of the environment: Review of health protective effects of nature and daylight, Applied Psychology: Health and Well-Being 6 (1) (2014) 67–95.

[6] J. Heerwagen, Green buildings, organizational success and occupant pro-ductivity, Building Research & Information 28 (5-6) (2000) 353–367.

[7] B. Thayer, Daylighting and productivity at lockheed, Solar Today 9 (3) (1995) 26–29.

[8] S. Tom, Managing energy and comfort, ASHRAE Journal 50 (6) (2008) 18–27.

[9] Comit´e Europ´een de Normalisation, En 12464-1: Light and lighting-lighting of work places, part 1: Indoor work places, Brussels: CEN, (2002).

[10] E. Mills, G. Bell, D. Sartor, D. Avery, M. Siminovitch, M. A. Piette, A design guide for energy-efficient research laboratories, in: LBNL-PUB-777, Lawrence Berkeley National Laboratory, Center for Building Sci-ence, Applications Team, Sept. 1996.

[11] S. Begemann, G. Van den Beld, A. Tenner, Daylight, artificial light and people in an office environment, overview of visual and biological responses, International Journal of Industrial Ergonomics 20 (3) (1997) 231–239.

[12] N. Baker, We are all outdoor animals, in: Architecture City Environment, Proceedings of PLEA, Vol. 2000, 2000, pp. 553–555.

[13] Comit´e Europ´een de Normalisation, prEN 17037: Daylight of buildings, Brussels: CEN, (2016).

[14] J. Wienold, J. Christoffersen, Evaluation methods and development of a new glare prediction model for daylight environments with the use of ccd cameras, Energy and buildings 38 (7) (2006) 743–757.

[15] R. G. Hopkinson, Glare from daylighting in buildings, Applied Ergonomics 3 (4) (1972) 206–215.

[16] K. V. D. Wymelenberg, M. Inanici, A critical investigation of common lighting design metrics for predicting human visual comfort in offices with daylight, LEUKOS 10 (3) (2014) 145–164.

[17] S. Carlucci, F. Causone, F. De Rosa, L. Pagliano, A review of indices for assessing visual comfort with a view to their use in optimization processes to support building integrated design, Renewable and sustainable energy reviews 47 (2015) 1016–1033.

[18] V. Gavan, M. Woloszyn, F. Kuznik, J.-J. Roux, Experimen-tal study of a mechanically ventilated double-skin fac¸ade with venetian sun-shading device: A full-scale investigation in con-trolled environment, Solar Energy 84 (2) (2010) 183 – 195. doi:https://doi.org/10.1016/j.solener.2009.10.017.

[19] J. Mardaljevic, R. K. Waskett, B. Painter, Electrochromic glazing in build-ings: A case study, Electrochromic Materials and Devices (2013) 571– 592.

[20] C. M. Lampert, Smart switchable glazing for solar energy and daylight control, Solar Energy Materials and Solar Cells 52 (3-4) (1998) 207–221.

[21] A. D. Galasiu, J. A. Veitch, Occupant preferences and satisfaction with the luminous environment and control systems in daylit offices: a literature review, Energy and Buildings 38 (7) (2006) 728–742.

[22] V. Inkarojrit, Monitoring and modelling of manually-controlled venetian blinds in private offices: a pilot study, Journal of Building Performance Simulation 1 (2) (2008) 75–89.

[23] A. Mahdavi, C. Proglh¨of,¨ User behavior and energy performance in build-ings, Wien, Austria: Internationalen Energiewirtschaftstagung an der TU Wien (IEWT) (2009) 1–13.

[24] A. Tzempelikos, A. K. Athienitis, The impact of shading design and con-trol on building cooling and lighting demand, Solar energy 81 (3) (2007) 369–382.

[25] R. Sullivan, E. S. Lee, K. Papamichael, M. Rubin, S. E. Selkowitz, Effect of switching control strategies on the energy performance of electrochromic windows, in: Optical Materials Technology for Energy Efficiency and Solar Energy Conversion XIII, Vol. 2255, International Society for Optics and Photonics, 1994, pp. 443–456.

[26] J. Karlsson, B. Karlsson, A. Roos, Control strategies and energy sav-ing potentials for variable transmittance windows versus static windows, Proc. of Eurosun, Copenhagen, Denmark, 2000.

[27] E. Lee, D. DiBartolomeo, S. Selkowitz, Daylighting control per-formance of a thin-film ceramic electrochromic window: Field study results, Energy and Buildings 38 (1) (2006) 30 – 44. doi:https://doi.org/10.1016/j.enbuild.2005.02.009.

[28] B. Roisin, M. Bodart, A. Deneyer, P. Dherdt, Lighting energy savings in offices using different control systems and their real consumption, Energy and Buildings 40 (4) (2008) 514–523.

[29] A. Jonsson, A. Roos, Evaluation of control strategies for different smart window combinations using computer simulations, Solar Energy 84 (1) (2010) 1 – 9. doi:https://doi.org/10.1016/j.solener.2009.10.021.

[30] F. Gugliermetti, F. Bisegna, Visual and energy management of electrochromic windows in mediterranean climate, Building and Environment 38 (3) (2003) 479 – 492. doi:https://doi.org/10.1016/S0360-1323(02)00124-5.

[31] A. Piccolo, F. Simone, Effect of switchable glazing on discomfort glare from windows, Building and Environment 44 (6) (2009) 1171–1180.

[32] A. A. Nazzal, A new daylight glare evaluation method: Introduction of the monitoring protocol and calculation method, Energy and Buildings 33 (3) (2001) 257–265.

[33] W. K. Osterhaus, I. L. Bailey, Large area glare sources and their effect on visual discomfort and visual performance at computer workstations, in: Industry Applications Society Annual Meeting, 1992., Conference Record of the 1992 IEEE, IEEE, 1992, pp. 1825–1829.

[34] M. Moeck, E. S. Lee, M. D. Rubin, R. Sullivan, S. E. Selkowitz, Vi-sual quality assessment of electrochromic and conventional glazings, in: SPIE Optical Materials Technology for Energy Efficiency and Solar En-ergy Conversion XV, Freiburg, Germany, 1996.

[35] R. Clear, V. Inkarojrit, E. Lee, Subject responses to electrochromic windows, Energy and Buildings 38 (7) (2006) 758–779.

[36] L. Fernandes, E. S. Lee, G. Ward, Lighting energy savings potential of split-pane electrochromic windows controlled for daylighting with visual comfort, Energy and Buildings 61 (2013) 8–20.

[37] L. L. Fernandes, E. S. Lee, A. Thanachareonkit, Electrochromic window demonstration at the donna land port of entry, Tech. rep., LBNL-1001788 (May 2015).

[38] C. Goovaerts, F. Descamps, V. Jacobs, Shading control strategy to avoid visual discomfort by using a low-cost camera: A field study of two cases, Building and Environment 125 (2017) 26–38.

[39] G. Newsham, C. Arsenault, A camera as a sensor for lighting and shading control, Lighting Research & Technology 41 (2) (2009) 143–163.

[40] J. Mardaljevic, R. Kelly Waskett, B. Painter, Neutral daylight illumination with variable transmission glass: Theory and validation, Lighting Research & Technology 48 (3) (2016) 267–285.

[41] Y. Wu, J. H. K¨ampf, J.-L. Scartezzini, Design and validation of a com-pact embedded photometric device for real-time daylighting comput-ing in office buildings, Building and Environment 148 (2019) 309–322. doi:https://doi.org/10.1016/j.buildenv.2018.11.016.

[42] Y. Wu, J. H. K¨ampf, J.-L. Scartezzini, An embedded system for quasi real-time lighting computation based on sky monitoring, in: Building Simula-tion, IBPSA San Francisco, California, 2017.

[43] Commission Internationale de l'Eclairage, CIE Proceedings 1924 (1926).

[44] Y. Wu, J. H. K¨ampf, J.-L. Scartezzini, Automated eye-sight vene-tian blinds based on an embedded photometric device with real-time daylighting computing, Applied Energy 252 (2019) 113317. doi:https://doi.org/10.1016/j.apenergy.2019.113317.

[45] Y. Wu, J. H. K¨ampf, J.-L. Scartezzini, Lighting simulation for external venetian blinds based on btdf and hdr sky luminance monitoring, in: 7th International Building Physics Conference, IBPC2018, Syracuse, NY, USA, 2018.

[46] G. W. Larson, R. Shakespeare, Rendering with Radiance: the art and science of lighting visualization, Booksurge Llc, 2004.

[47] M. Pharr, W. Jakob, G. Humphreys, Physically based rendering: From theory to implementation, Morgan Kaufmann, 2016.

[48] G. Ward, R. Mistrick, E. S. Lee, A. McNeil, J. Jonsson, Simulating the daylight performance of complex fenestration systems using bidirectional scattering distribution functions within radiance, Leukos 7 (4) (2011) 241–261.

[49] A. McNeil, The five-phase method for simulating complex fenestration with radiance, Lawrence Berkeley National Laboratory, Berkeley, CA, USA (2013) 1–23.

[50] E. S. Lee, D. Geisler-Moroder, G. Ward, Modeling the direct sun compo-nent in buildings using matrix algebraic approaches: Methods and valida-tion, Solar Energy 160 (2018) 380–395.

[51] P. R. Tregenza, Subdivision of the sky hemisphere for luminance measurements, Lighting Research & Technology 19 (1) (1987) 13–14.

[52] J. H. Klems, J. L. Warner, Measurement of bidirectional optical properties of complex shading devices, ASHRAE Transactions 101-1.

[53] F. Bartell, E. Dereniak, W. Wolfe, The theory and measurement of bidirectional reflectance distribution function (brdf) and bidirectional transmittance distribution function (btdf), in: Radiation scattering in optical systems, Vol. 257, International Society for Optics and Photonics, 1981, pp. 154–161.

[54] I. Konstantzos, A. Tzempelikos, Y.-C. Chan, Experimental and simulation analysis of daylight glare probability in offices with dynamic window shades, Building and Environment 87 (2015) 244–254.

[55] A. Nabil, J. Mardaljevic, Useful daylight illuminances: A replacement for daylight factors, Energy and buildings 38 (7) (2006) 905–913.

[56] J. Mardaljevic, M. Andersen, N. Roy, J. Christoffersen, Daylighting met-rics: is there a relation between useful daylight illuminance and daylight glare probabilty?, in: Proceedings of the building simulation and opti-mization conference BSO12, no. CONF, 2012.

[57] R. Perez, R. Seals, J. Michalsky, All-weather model for sky luminance distributionpreliminary configuration and validation, Solar energy 50 (3) (1993) 235–245.